Order and disorder in calcium–silicate–hydrate

M. Bauchy, M. J. Abdolhosseini Qomi, F.-J. Ulm, and R. J.-M. Pellenq

Citation: The Journal of Chemical Physics **140**, 214503 (2014); doi: 10.1063/1.4878656

View online: http://dx.doi.org/10.1063/1.4878656

View Table of Contents: http://scitation.aip.org/content/aip/journal/jcp/140/21?ver=pdfcov

Published by the AIP Publishing

Order and disorder in calcium–silicate–hydrate

M. Bauchy,[1,2,a] M. J. Abdolhosseini Qomi,[1] F.-J. Ulm,[1] and R. J.-M. Pellenq[1,2,3]
[1]*Concrete Sustainability Hub, Department of Civil and Environmental Engineering, Massachusetts Institute of Technology, 77 Massachusetts Avenue, Cambridge, Massachusetts 02139, USA*
[2]*MIT-CNRS Joint Laboratory at Massachusetts Institute of Technology, 77 Massachusetts Avenue, Cambridge, Massachusetts 02139, USA*
[3]*Centre Interdisciplinaire des Nanosciences de Marseille, CNRS and Aix-Marseille University, Campus de Luminy, 13288 Marseille Cedex 09, France*

(Received 11 March 2014; accepted 2 May 2014; published online 3 June 2014)

Despite advances in the characterization and modeling of cement hydrates, the atomic order in Calcium–Silicate–Hydrate (C–S–H), the binding phase of cement, remains an open question. Indeed, in contrast to the former crystalline model, recent molecular models suggest that the nanoscale structure of C–S–H is amorphous. To elucidate this issue, we analyzed the structure of a realistic simulated model of C–S–H, and compared the latter to crystalline tobermorite, a natural analogue of C–S–H, and to an artificial ideal glass. The results clearly indicate that C–S–H appears as amorphous, when averaged on all atoms. However, an analysis of the order around each atomic species reveals that its structure shows an intermediate degree of order, retaining some characteristics of the crystal while acquiring an overall glass-like disorder. Thanks to a detailed quantification of order and disorder, we show that, while C–S–H retains some signatures of a tobermorite-like layered structure, hydrated species are completely amorphous. © *2014 AIP Publishing LLC*. [http://dx.doi.org/10.1063/1.4878656]

I. INTRODUCTION

Calcium–silicate–hydrate (C–S–H) is the main hydration product in cementitious systems and acts as the binding phase in the paste.[1] It is thus responsible for its strength, durability, and creep properties.[2] Following a bottom-up approach, the knowledge of the molecular structure of C–S–H is a required input to any upscaling model.

Despite its ubiquitous presence in the built environment, the structure of C–S–H at the nanoscale remains controversial. As X-ray diffraction patterns from C–S–H have shown to exhibit only a few broad and weak diffraction maxima, it has been described as an amorphous material.[3–5] However, most experimental studies[6–12] suggest that its structure is close to that of tobermorite, although their compositions differ. Hence, it is still unclear whether C–S–H should be considered as a crystalline or an amorphous material. Fortunately, a realistic atomistic model of C–S–H has recently been reported,[9,13–16] thus opening the way to elucidate its nature.

To quantify the atomic order in C–S–H, we analyzed the previously mentioned atomistic model. We compared its structure with the one of tobermorite,[17] its crystal analogue, while taking care to rescale the results to account for the difference of composition (see below). The structure was also compared with that of an ideal artificial glass, formed by quickly heating and cooling a C–S–H system. Through the consistent structural analysis of those three systems, simulated in the same conditions and with the same potential, we were able to assess their relative atomic order both at the short- and medium-range order. Eventually, for the three considered systems, we quantified the disorder around each species in the atomic network by calculating total and partial excess entropy.

This article is organized as follows. In Sec. II, we present the numerical model and methodology that we used to simulate C–S–H and the corresponding crystal and glass. In Sec. III, we focus on the glass transition observed during the fast cooling of the system. We analyze the atomic structure of C–S–H as compared with the ones of the crystal and the glass, respectively, at the short- and medium-range order in Secs. IV and V. Those results are discussed in Sec. VI, in which we quantify the relative order in the atomic configurations of C–S–H, the crystal and the glass. Concluding remarks are presented in Sec. VII.

II. METHODS

In this section, we detail the model and the procedure used to simulate C–S–H and its crystalline and glassy analogue.

A. A realistic model of C–S–H

To describe the disordered molecular structure of C–S–H, Pellenq *et al.*[18] proposed a realistic model for C–S–H with the stoichiometry of $(CaO)_{1.65}(SiO_2)(H_2O)_{1.73}$. We generated the C–S–H model by introducing defects in an 11 Å tobermorite[17] configuration, following a combinatorial procedure. An 11 Å tobermorite consists of pseudo-octahedral calcium oxide sheets, which are surrounded by silicate tetrahedral chains. The latter consists of bridging oxygen atoms and Q^2 silicon atoms (having two bridging and two

[a]Author to whom correspondence should be addressed. Electronic mail: bauchy@mit.edu. URL: http://mathieu.bauchy.com. Present address: Department of Civil and Environmental Engineering, University of California, Los Angeles, California 90095, USA.

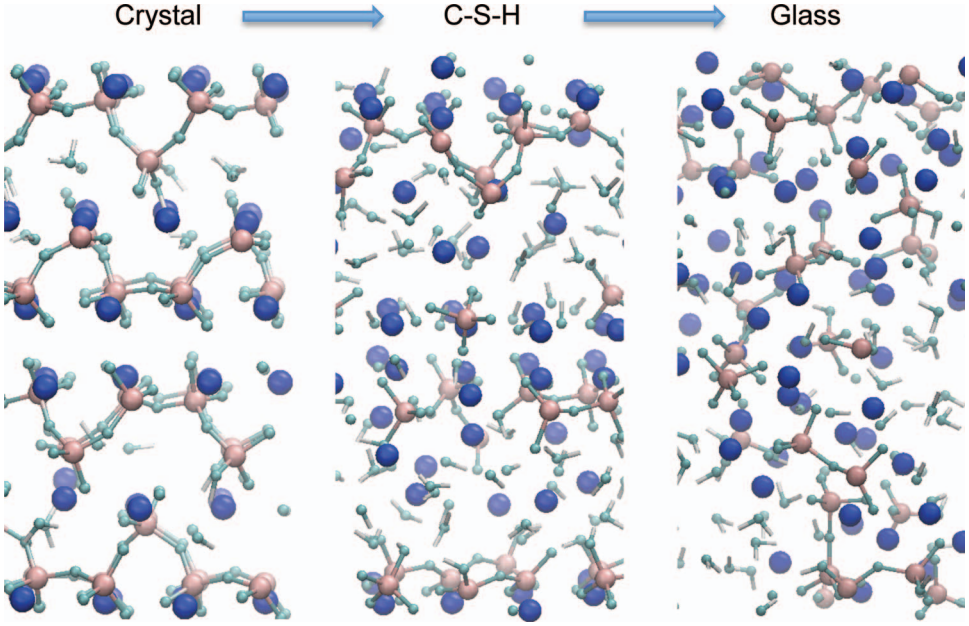

FIG. 1. Snapshots of the atomic configurations of the simulated tobermorite, C–S–H and artificial glass.

non-bridging terminal oxygen atoms).[19] Those negatively charged calcium–silicate sheets are separated from each other by an interlayer spacing, which contains interlayer water molecules and charge-balancing calcium cations. Although the Ca/Si ratio in 11 Å tobermorite is 1, this ratio is increased to 1.65 in the present C–S–H model through randomly removing SiO_2 groups.

The defects in the silicate chains provide possible sites for adsorption of extra water molecules. The adsorption of water molecules in the structurally defected tobermorite model was performed via the Grand Canonical Monte Carlo method, ensuring equilibrium with bulk water at constant volume and room temperature. The REAXFF potential,[20] a reactive potential, was then used to account for the reaction of the interlayer water with the defective calcium–silicate sheets. The use of this reactive potential allows the water molecules to dissociate into hydroxyl groups. More details on the preparation of the model and its experimental validation can be found elsewhere.[14–16,21]

B. Simulation of C–S–H

Relying on the previously presented model, we simulated a C–S–H box made of 501 atoms. We used molecular dynamics, implemented thanks to the LAMMPS package.[22] To this end, we used the REAXFF potential[20] with a time-step of 0.25 fs. We first relaxed the system at zero pressure and 300 K during 2.5 ns in the NPT ensemble and made sure that the convergence of the energy and volume was achieved. Subsequently, we ran a 25 ps simulation in the NVT ensemble for statistical averaging. Figure 1 shows a snapshot of the atomic configuration of the C–S–H model.

C. Simulation of the crystal analogue

We chose to study 11 Å tobermorite as it is considered a natural crystal analogue for C–S–H (see Sec. I). This choice was also motivated by the fact that the simulated C–S–H sample was prepared by introducing defects in the silicate chains of tobermorite.

For consistent comparison with C–S–H, this system was simulated using the REAXFF potential, i.e., the same as the one we used for C–S–H, the same time-step and following the same procedure. We started from a supercell of 11 Å tobermorite[17] composed of 288 atoms and relaxed it at zero pressure and 300 K during 2.5 ns in the NPT ensemble. We checked the convergence of the volume and the energy and ran a 25 ps simulation in the NVT ensemble for statistical averages. Note that the use of the REAXFF potential does not induce any significant change of volume or structural modification with respect to the starting configuration.[17] In particular, no further dissociation of the water molecules is observed. A snapshot of the final configuration is presented in Figure 1.

It should be noted that 11 Å tobermorite does not have the same composition or density as C–S–H. In particular, its Ca/Si ratio is 1, whereas the one of C–S–H is 1.65. To compare the results with C–S–H, we rescaled all the computed properties to take this difference into account. In practice, this is achieved by replacing the concentration of every species by the ones in C–S–H. In the following, we will refer to the rescaled results obtained for tobermorite as being the properties of the *crystal*.

D. Simulation of the glass analogue

Here, we aim to compare the structure of C–S–H with that of an ideal glass. To this end, we created an artificial glass analogue of C–S–H by heating and cooling the previous C–S–H configuration. This methodology is commonly used to simulate glassy materials; e.g., one usually prepares glassy silica by heating and cooling quartz.[23]

We started from the relaxed configuration of C–S–H. The system was then instantly heated to 3000 K and relaxed

during 2.5 ns at constant pressure in the NPT ensemble at this temperature, which is well above the melting temperature of calcium–silicate systems (for example, 1813 K for the dicalcium silicate crystal[24]). This allowed the system to lose the memory of its initial configuration. We checked this by computing the root-mean-square displacement of each species and making sure that, at the end of the simulation, they were far larger than the size of the simulation box. The system was then gradually cooled from 3000 K down to 300 K in the NPT ensemble, with a cooling rate q of 20, 40, and 80 K/ps. During the melting and cooling phases, we imposed a pressure of 0.1 GPa to prevent water molecules to leave the system at high temperature, which would lead to artificially large simulation box. However, this pressure is small as compared to the large pressure fluctuations in the system due to its small size (typically around 1 GPa). Therefore, we do not expect this pressure to have any significant impact on the structure of the simulated glass. More details about the glass transition undergone by the system during the cooling phase are presented in Sec. III. At 300 K, the obtained glass was relaxed in the NPT ensemble at zero pressure for 2.5 ns. At this stage, we checked the convergence of the energy and volume of the system. Eventually, we ran a 25 ps simulation in the NVT ensemble at 300 K for statistical averaging.

The final configuration of the glass is shown in Figure 1. We note that the local environment of the atoms does not change significantly from that of C–S–H and tobermorite (e.g., one finds 4-fold coordinated silicon atoms). Interestingly, the fraction of dissociated/undissociated water molecules in the glass is similar to that in C–S–H. The obtained glass is not homogeneous, as we find some clusters of undissociated water molecules, thus suggesting that the system tend to demix. This means that such a high concentration of water in a calcium silicate glass might not be realistic. However, we do not aim to simulate a realistic glass: we only consider this system as an artificial material, allowing to compare C–S–H with a perfectly disordered system of the same chemistry.

Note that the volume of the simulation box increases by 80% when heated to 3000 K. However, after being cooled, the volume of the system goes back to a value fairly close to the volume of the initial C–S–H box (larger by 3%). Once again, to allow for a consistent comparison with C–S–H, we used the same REAXFF potential and the same time-step during the entire procedure. In the following, we will refer to the results obtained for this system as being the properties of the *glass*. By construction, this system has the same composition as the C–S–H model, so that no rescaling is needed.

III. GLASS TRANSITION

We first focus on the glass formation in the C–S–H system. The inset of Figure 2 shows the volume V of the system, normalized by one of the final glasses, with respect to temperature T, during the cooling phase. The glass transition manifested with a change in the slope of $V(T)$, as typically observed in silicate glasses.[25] The glass transition temperature T_g can be determined from the cross-point of the high- and low-temperature extrapolation of $V(T)$. We found $T_g = 1098$ K with a cooling rate of 20 K/ps.

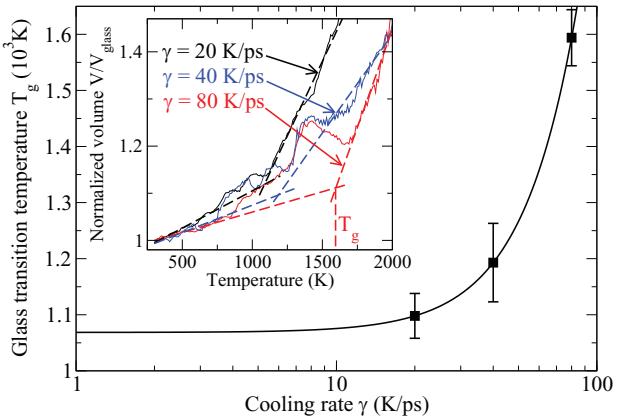

FIG. 2. Glass transition temperature as a function of the cooling rate. The inset shows the volume, normalized by one of the final glasses, with respect to temperature, for selected cooling rates at constant pressure. The change of slope allows identifying the value of the glass transition temperature for each cooling rate.

Such a cooling rate is obviously far larger than the ones typically used in the lab (around 100 K/s at most). However, high cooling rate is an intrinsic limit of molecular dynamics simulations, due to their high computational cost. To be able to extrapolate the obtained T_g to usual lab conditions, we performed two additional quenchings using cooling rates of 40 and 80 K/ps. Figure 2 shows the evolution of T_g as a function of the cooling rate q. In the case of silica, based on the mode-coupling theory of the glass transition, it was reported[26] that T_g increases with q, following the formula:

$$T_g(q) = T_c + (Aq)^{1/\delta}, \tag{1}$$

where T_c, A, and δ are fitting parameters, with no clear physical origin. As shown in Figure 2, the values of T_g obtained for the C–S–H system are fairly well fitted by this law. This allows us to extrapolate T_g up to reasonable cooling rates. For cooling rates lower than 1 K/ps, T_g shows a plateau value of 1067 K. This value can be compared with $T_g = 1085$ K[27] in the case of a calcium aluminosilicate glass, with a Ca/Si of 1.6, fairly similar to the value of 1.65 used in the present C–S–H model. The temperature is well below the typical melting temperature of calcium–silicate crystals, so that we obtain a supercooled liquid before the glass transition. Hence, we feel confident that the structure of the quenched system is representative of an ideal glass.

IV. SHORT-RANGE ORDER

A. Preliminary observations

A direct observation of the atomic snapshots of the obtained C–S–H, crystal and glass (see Figure 1) reveals that C–S–H appears to have a structure intermediate between one of the crystals and one of the glasses. Indeed, despite a layered structure somehow retained in C–S–H, the latter structure shows an increased disorder with respect to the crystal. In the following, we aim to quantify the relative order of those systems.

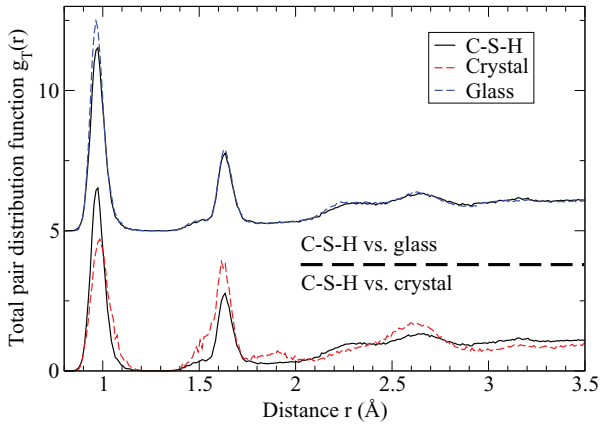

FIG. 3. Total pair distribution function of C–S–H compared with the ones for the corresponding glass (top) and crystal (bottom).

B. Total pair distribution function

As a first step, we computed the total pair distribution function (PDF) $g_T(r)$ of the three systems from the knowledge of the partial PDF $g_{ij}(r)$,

$$g_T(r) = \sum_{i,j=1}^{n} c_i c_j g_{ij}(r), \tag{2}$$

where c_i is the fraction of i atoms (Si, Ca, H, or O). Note that, to allow for a consistent comparison, we use the c_i factors obtained for C–S–H to compute the PDF of the crystal.

Figure 3 shows the total PDFs of C–S–H, compared with one of the crystals and glasses. We note that the PDFs of those three systems do not show significant differences that would clearly allow distinguishing a glassy from a crystalline phase. They actually present a shape similar to the PDFs of silicate[28] and chalcogenide glasses.[29] The first peak in the 1 Å region is associated with H–O bonds. The second peak in the 1.6 Å region corresponds to a superposition of the H–H and Si–O correlations. The following peaks are not easily distinguishable as they are a result of the superposition of several contributions from different pairs of atoms. Overall, we observe a closer agreement of the PDF of C–S–H with one of the glasses than with one of the crystals. This tends to show that the structure of C–S–H is mostly amorphous when averaged on all pairs of atoms.

C. X-ray pair distribution function

To compare these PDFs to those obtained via x-ray diffraction, we computed the x-ray PDFs,

$$g_X(r) = \frac{1}{\sum_{i,j=1}^{n} c_i c_j b_i b_j} \sum_{i,j=1}^{n} c_i c_j b_i b_j g_{ij}(r), \tag{3}$$

where b_i is the x-ray scattering length for i atoms, which we assumed to be constant as in Ref. 30. Note that, to take into account the maximal scattering vector Q_{max} of the experimental structure factor, the computed PDFs were broadened by following the methodology described in Refs. 31 and 32.

Figure 4 shows the x-ray PDFs of C–S–H, glass, and crystal, compared with experimental data obtained by

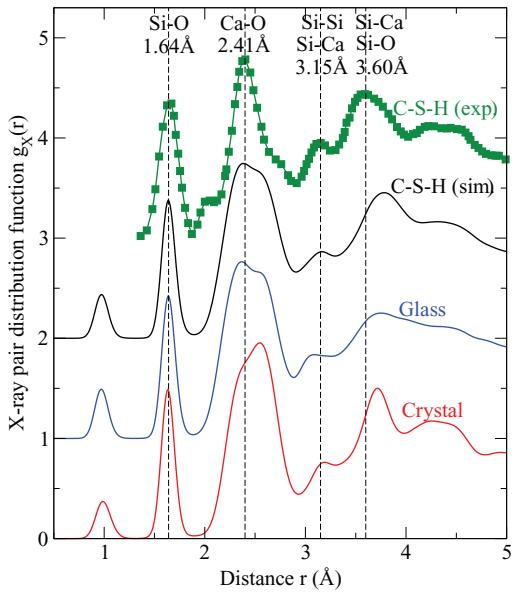

FIG. 4. X-ray pair distribution function of C–S–H compared with the ones for the corresponding glass and crystal. Experimental data for an artificial C–S–H with Ca/Si = 1.6[30] is shown for comparison.

Monteiro *et al.*[9,10,30] for an artificial C–S–H specimen with Ca/Si = 1.6, fairly similar to the present composition. First, we note a good agreement between simulation and experiment for C–S–H, which is remarkable considering the complexity of the material. In particular, the positions and heights of the first peaks, associated with Si–O, Ca–O, and Si–Si correlations, respectively, are well reproduced by the simulation. Although the general shape at high r is also well reproduced, we observe a slight shift of the Si–Ca peak. Second, we realize that the PDF is not a discriminant tool to characterize a structure. Indeed, the general shape of the experimental PDF is fairly similar to those of the glass and the crystal. However, we note that the Ca–O peak for the crystal is shifted from 2.41 Å to 2.55 Å. The local-range order of the glass is similar to that of C–S–H, but we observe that the structure at the medium-range order is less ordered, as the peaks become less intense than in C–S–H.

The x-ray PDF of C–S–H differs from that of the glass, whereas, as mentioned, the total PDFs are similar. Since the x-ray PDF is characterized by a different weight for each pair of atom, captured by the scattering lengths, this suggests that, to fully characterize the degree of order and disorder in C–S–H, one has to consider the partial contribution of each pair of atoms. This is the focus of Secs. IV D–VI of the paper.

D. Partial pair distribution function

To better characterize the local structure in C–S–H, we computed all the partial PDFs. Selected partial PDFs are shown in Figure 5. Note that O_w refers to oxygen atoms belonging to water molecules. First, we note that the present PDFs of C–S–H fairly correspond to that of Pellenq *et al.*,[18] although the core-shell potential that was used did not take into account the reactivity of the water molecules. In particular, the Ca–O partial does not show any significant change.

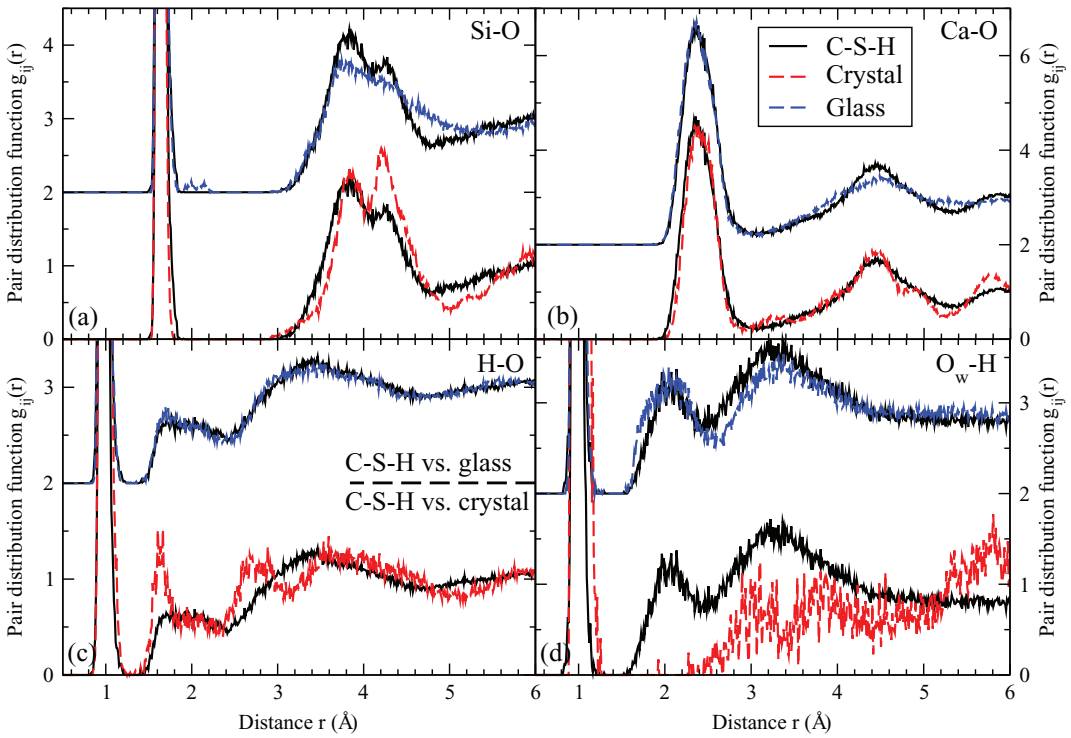

FIG. 5. Partial distribution functions for the (a) Si–O, (b) Ca–O, (c) H–O, and (d) O_w–H pairs, where O_w refers to oxygen atoms in water molecules. For each pair, the partial distribution function of C–S–H is compared with one of the corresponding glasses (top) and one of the crystals (bottom).

The present Si–O partial shows an additional small peak at 4.3 Å, but remains fairly unchanged for other *r*.

Figures 5(a) and 5(b) show that the short-range order of Si and Ca atoms is roughly similar in the crystal, in C–S–H and in the glass. In particular, the position and integral of the first peak do not show any significant change, which means that the atomic bond distance Si–O and Ca–O as well as the coordination number of the cations are the same. This is not surprising, as glasses typically tend to retain the same local order as observed in the corresponding crystal.

However, some differences start to appear at a larger scale. The second coordination shell peak of the Si–O partial PDF of C–S–H shows a bimodal distribution, which is reminiscent of the one observed in the crystal. On the contrary, the glass only shows a smooth broad peak corresponding to the second coordination shell. This means that a certain degree of order is maintained in the silicate layers in C–S–H. In the case of the Ca–O partial, the PDF of the crystal shows a small peak around 3.2 Å, which disappears in C–S–H. However, the peaks observed in the PDF of the glass are broader than the ones of C–S–H. Overall, C–S–H seems to present an atomic order that is intermediate between the ones of the crystal and the glass in the Si and Ca local environment.

On the contrary, the environment of hydroxyl groups [Figure 5(c)] and water molecules [Figure 5(d)] show a different behavior. Once again, the first peak is fairly similar in C–S–H, in the crystal and in the glass, corresponding to similar bond distances and coordination numbers. However, structural correlations at a larger scale ($r > 1.5$ Å) appear to be almost identical in C–S–H and in the glass, and significantly different from the ones observed in the crystal. This is clear evidence that the disorder observed inside C–S–H, when averaged on all atoms, mainly arises from water molecules and hydroxyl groups. In particular, the O_w–H partial show a peak around 2 Å for C–S–H and the glass. This arises from the existence of hydrogen bonds between water molecules and/or hydroxyl groups. This feature is not observed in the crystal as the water molecules are well separated from each other.

Since the structural differences between C–S–H, the glass, and the crystal seem to appear at scales larger than one of the first coordination shells, we analyzed second neighbor cation–cation and water–water correlations. Overall, the first peaks of the Si–Si [Figure 6(a)] and Ca–Ca [Figure 6(b)] partial PDFs of C–S–H are systematically broader than in the crystal, but sharper than in the glass. This confirms the fact that the calcium and silicate layers in C–S–H retain some crystal-like order, as opposed to H–H [Figure 6(c)] and water–water [Figure 6(d)] correlations, which are essentially amorphous. Since the weight associated to H atoms is small in x-ray scattering, C–S–H tends to appear more crystalline with these experiments than when averaged equally on all pairs of atoms.

V. MEDIUM-RANGE ORDER

As we realized that the local environment of the different species was not enough to distinguish the order in C–S–H from one of the crystals and one of the glasses, we analyzed the medium range order (MRO) of those systems by computing the neutron structure factor. The partial structure factors

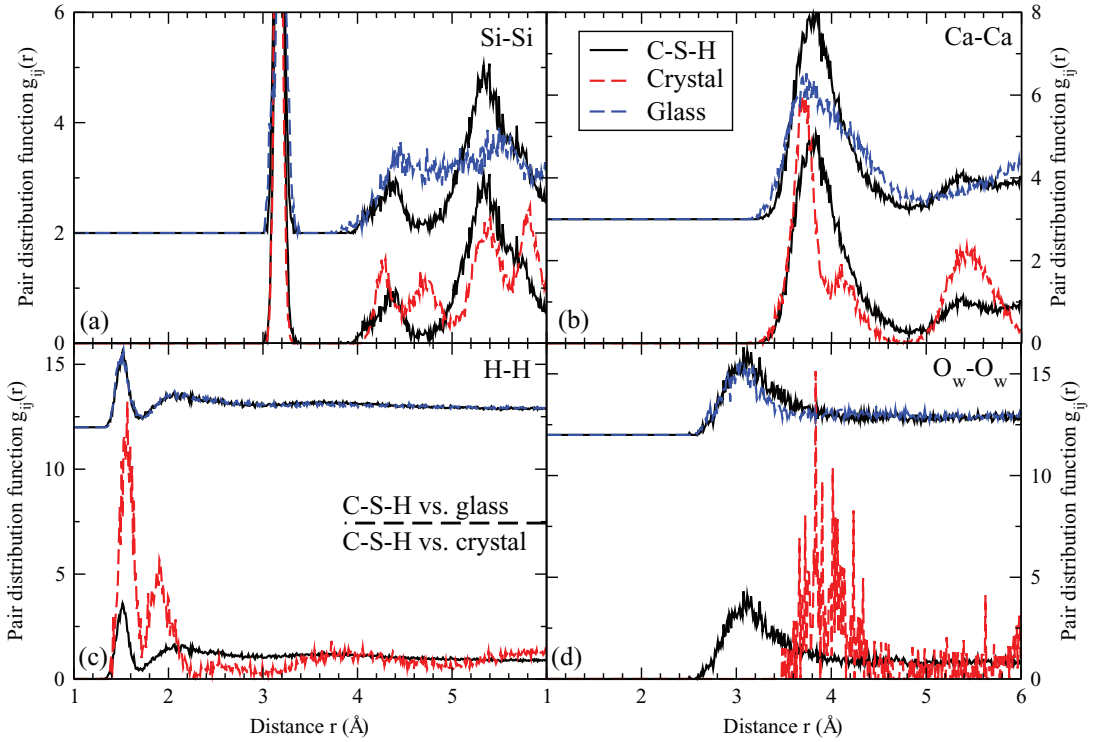

FIG. 6. Partial distribution functions for the (a) Si–Si, (b) Ca–Ca, (c) H–H, and (d) O_w–O_w pairs, where O_w refers to oxygen atoms in water molecules. For each pair, the partial distribution function of C–S–H is compared with one of the corresponding glasses (top) and one of the crystals (bottom).

were first calculated from the pair distribution functions $g_{ij}(r)$,

$$S_{ij}(Q) = 1 + \varrho_0 \int_0^R 4\pi r^2 (g_{ij}(r) - 1) \frac{\sin(Qr)}{Qr} F_L(r)\, dr, \quad (4)$$

where Q is the scattering wave vector, ϱ_0 is the average atom number density, and R is the maximum value of the integration in real space (here, $R = 6$ Å). The $F_L(r) = \sin(\pi r/R)/(\pi r/R)$ term is a Lorch-type window function, used to reduce the effect of the finite cutoff of r in the integration.[33] As discussed in Ref. 34, the use of this function reduces the ripples at low Q, but induces a broadening of the structure factor peaks. The total neutron structure factor can then be evaluated from the partial structure factors following:

$$S_N(Q) = \left(\sum_{i,j=1}^{n} c_i c_j b_i b_j \right)^{-1} \sum_{i,j=1}^{n} c_i c_j b_i b_j S_{ij}(Q), \quad (5)$$

where c_i is the fraction of i atoms (Si, Ca, H, or O) and b_i is the neutron scattering length of the species (given by 4.1491, 4.70, –3.7390, and 5.803 fm for silicon, calcium, hydrogen, and oxygen atoms, respectively[35]). Once again, note that, to allow for a consistent comparison, we use the c_i factors obtained for C–S–H for the crystal.

A. Neutron structure factor

Figure 7 shows the total neutron structure factor for C–S–H as well as for the corresponding crystal and glass. Once again, the three structure factors do not show significant differences and are typical of those observed in silicate[36] and chalcogenide[37] glasses. It should be mentioned that the limited sizes of the simulated systems do not allow us to study large-scale correlations (large r, low Q). Focusing on the low Q region of the structure factor, we note that the peaks show the same position in C–S–H and in the glass, although they appear sharper in C–S–H, which is a signature of an increased order on the MRO. On the contrary, the peaks at low Q do not show the same positions in C–S–H and in the crystal. Since each peak is a signature of a typical spatial repetition distance in the MRO,[37] it appears that the atomic order at the intermediate length scale of C–S–H is amorphous, when averaged on all pairs of atoms. In particular, we observe a

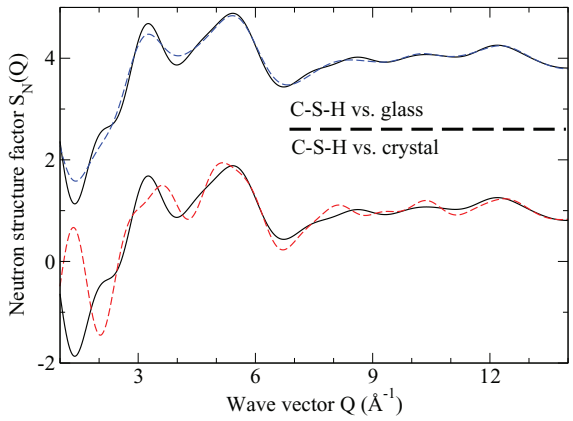

FIG. 7. Total neutron structure factor of C–S–H, compared with one of the corresponding glasses (top) and one of the crystals (bottom).

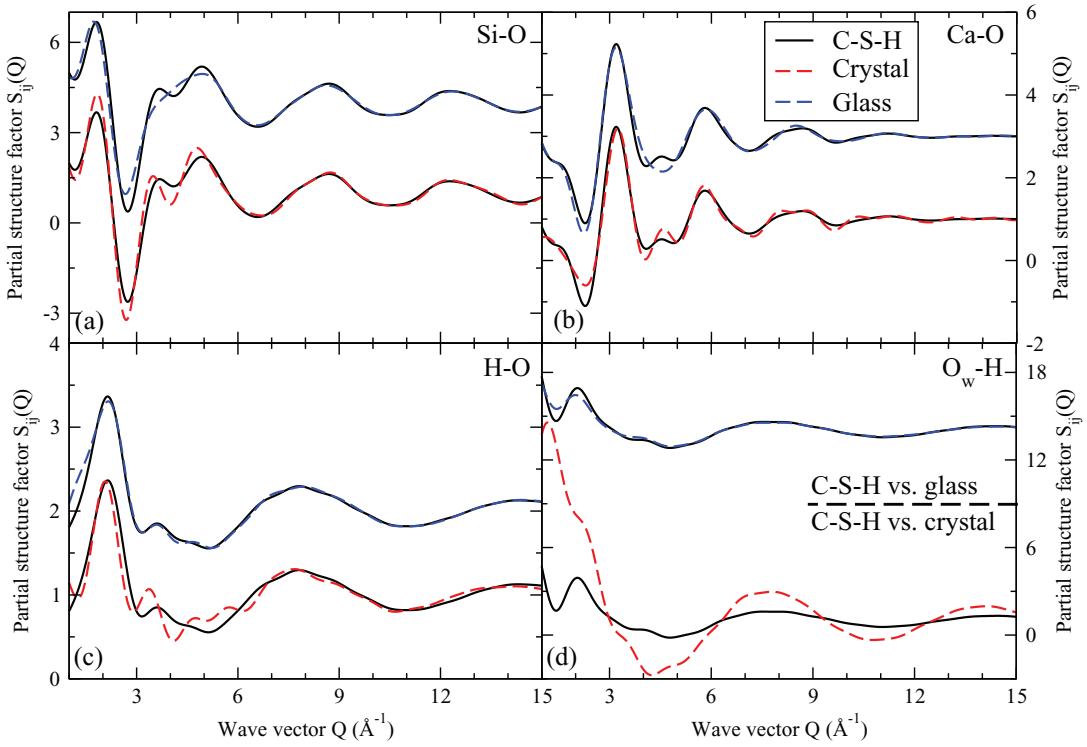

FIG. 8. Partial structure factors for the (a) Si–O, (b) Ca–O, (c) H–O, and (d) O_w–H pairs, where O_w refers to oxygen atoms in water molecules. For each pair, the partial structure factor of C–S–H is compared with one of the corresponding glasses (top) and one of the crystals (bottom).

first sharp peak around 1.5 $Å^{-1}$ for the crystal, arising from a strong order at large r, which is absent in C–S–H and the glass.

B. Partial structure factors

Similar to the case of the total PDF, the apparent disorder observed in the total structure factor actually results from some order and some disorder for different pairs of species. This is what we investigated by studying the decomposition of the total structure factor in the contributions of each partial (see Figures 8 and 9). The conclusions actually appear to be the same as those in Sec. VI. The MRO observed in calcium and silicate layers (tracked in the Si–O, Ca–O, Si–Si, and Ca–Ca partials) for C–S–H appears to be intermediate between one of the glasses and one of the crystals. In particular, Si–O, Ca–O, and Si–Si partials, respectively, show peaks around 3.5, 4.5, and 3.5 $Å^{-1}$, for both C–S–H and the crystal, which are absent in the case of the glass. On the contrary, partials associated with water and hydroxyl groups are almost identical for C–S–H and the glass, and significantly different from those observed in the crystal. Hence, the disorder observed in the medium-range order of C–S–H, when averaged on all pairs of atoms, is mainly caused by these hydration species.

VI. DISCUSSION

To study the relative atomic order in different systems, an excess entropy s_2 can easily be evaluated from the knowledge of the pair distribution functions. At the first order, one can calculate this quantity in using the expression of the two-body term,[38,39] which writes:

$$s_2 = -\frac{k_B \rho}{2} \sum_i \sum_j x_i x_j \int [g_{ij} \ln g_{ij} - (g_{ij} - 1)] d\mathbf{r}, \quad (6)$$

ρ being the density and x_i the concentration of species i. s_2 would be zero in an ideal gas where g_{ij}=1. Once again, note that, for a consistent comparison, we use the x_i factors of C–S–H for the crystal. A straightforward analysis of Eq. (6) shows that, the more peaked is g_{ij}, i.e., the more ordered is the system, the lower s_2 is. Hence, s_2 offers a practical way to quantify the order in a system and was used to compare the atomic structure of C–S–H with the corresponding crystal and glass. Note that, in the case of tobermorite, we used the atomic concentration and the density of C–S–H in Eq. (6) to get a meaningful comparison.

Results of this calculation are shown in the left part of Figure 10. As expected, s_2 is systematically larger in the glass than in the crystal due to the increased disorder. Interestingly, when averaged over all the pairs of atoms, the excess entropy of C–S–H appears to be intermediate between those two limits, but significantly closer to one of the glasses than to that of the crystals (respectively, –55.8, –45.8, and –43.3 J/K/mol in the crystal, in C–S–H, and in the glass). This strongly supports the idea that C–S–H can be seen as an amorphous material rather than a crystalline one, when averaged on all pairs of atoms.

To gain deeper insight into this apparent disorder, we computed the contribution to s_2 of each pair of atoms,

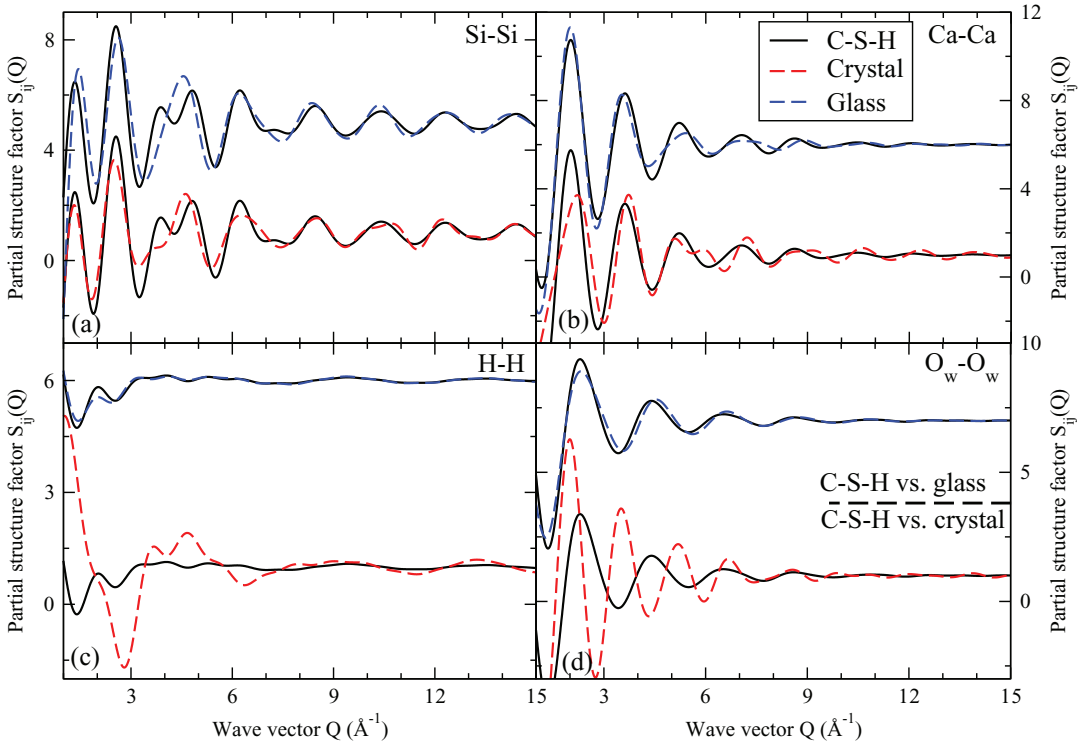

FIG. 9. Partial structure factors for the (a) Si–Si, (b) Ca–Ca, (c) H–H, and (d) O_w–O_w pairs, where O_w refers to oxygen atoms in water molecules. For each pair, the partial structure factor of C–S–H is compared with one of the corresponding glasses (top) and one of the crystals (bottom).

defined as

$$s_{2ij} = -\frac{k_B \rho}{2} x_i x_j \int [g_{ij} \ln g_{ij} - (g_{ij} - 1)] d\mathbf{r}. \qquad (7)$$

Results are shown in the right part of Figure 10. Once again, the excess entropy of C–S–H is systematically in between those of the crystal and the glass. However, its behavior appears to differ according to the considered pair of atoms. The values of the excess entropy associated with Ca–Ca and Si–Si pairs in C–S–H are closer to those obtained in the crystal than in the glass; whereas the opposite behavior is observed in the cases of the H–H and O_w–O_w partials. Hence, it is clear that calcium and silicate layers, while showing an increased disorder, retain some signature of a crystalline shape, whereas the distribution of the water molecules and the hydroxyl groups is amorphous.

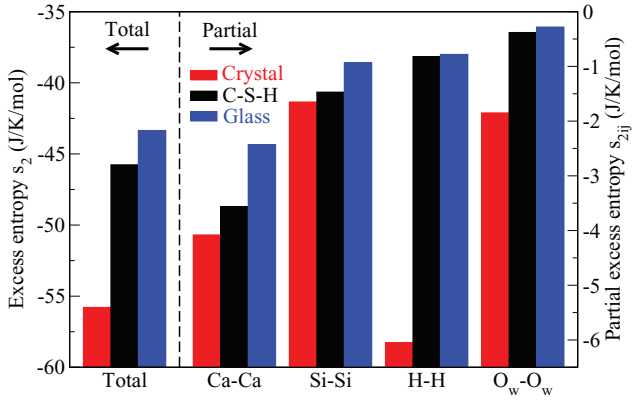

FIG. 10. Total (left) and partial (right) molar excess entropy for the crystal, C–S–H, and the glass.

VII. CONCLUSION

A detailed comparison of the structure of C–S–H, as well as those of the corresponding crystal and glass, has allowed us to better quantify the atomic order inside the binding phase of the cement paste. Overall, when averaged on all atoms, it appears that the structure of C–S–H is closer to a glass than that of a crystal. However, some atomic order, reminiscent of one of the crystals, is still found, although it is systematically in between the perfect order of a crystal and the perfect disorder of a glass. This manifests by a fairly layered structure, by silicate chains that are not completely amorphous, and by a non-random distribution of calcium atoms. On the contrary, water molecules and hydroxyl groups show a completely glassy spatial distribution, which suggests that these hydration species are more sensitive to the defects of the structure than the network formers species Si and Ca.

Hence, the atomic order of C–S–H can be qualified as being intermediate, definitely not fully crystalline, but not perfectly amorphous. The combination of a layered structure with an overall disorder may explain the paradoxical observation of an ordered or disordered structure, according to the experimental technique that is used.[12] Indeed, when averaged on all pairs of atom, C–S–H appears to be fully glassy. Thus, only the experiments providing an access to the detail of the order and disorder around each species would be able to capture the complexity of C–S–H.

ACKNOWLEDGMENTS

This work has been carried out within the framework of the ICoME2 Labex (ANR-11-LABX-0053) and the A*MIDEX projects (ANR-11-IDEX-0001-02) cofunded by the French program "Investissements d'Avenir" which is managed by the ANR, the French National Research Agency.

[1]H. F. W. Taylor, *Cement Chemistry* (Thomas Telford Publishing, 1997).
[2]M. Vandamme, F.-J. Ulm, and P. Fonollosa, Cem. Concr. Res. **40**, 14–26 (2010).
[3]E. Gartner, K. Kurtis, and P. Monteiro, Cem. Concr. Res. **30**, 817 (2000).
[4]X. Cong, N. Xu, R. J. Kirkpatrick, and G. E. Brown, Adv. Cem. Res. **9**, 31 (1997).
[5]P. Mandaliev, R. Dähn, J. Tits, B. Wehrli, and E. Wieland, J. Colloid Interface Sci. **342**, 1 (2010).
[6]X. Cong and R. Kirkpatrick, Adv. Cem. Based Mater. **3**, 144 (1996).
[7]A. J. Allen and J. J. Thomas, Cem. Concr. Res. **37**, 319 (2007).
[8]G. W. Groves, MRS Online Proc. Libr. **85**, 3 (1986).
[9]L. B. Skinner, S. R. Chae, C. J. Benmore, H. R. Wenk, and P. J. M. Monteiro, Phys. Rev. Lett. **104**, 195502 (2010).
[10]C. Meral, C. J. Benmore, and P. J. M. Monteiro, Cem. Concr. Res. **41**, 696 (2011).
[11]S. Grangeon, F. Claret, C. Lerouge, F. Warmont, T. Sato, S. Anraku, C. Numako, Y. Linard, and B. Lanson, Cem. Concr. Res. **52**, 31 (2013).
[12]S. Grangeon, F. Claret, Y. Linard, and C. Chiaberge, Acta Crystallogr., Sect. B: Struct. Sci., Cryst. Eng. Mater. **69**, 465 (2013).
[13]R. J.-M. Pellenq, N. Lequeux, and H. van Damme, Cem. Concr. Res. **38**, 159–174 (2008).
[14]M. Abdolhosseini Qomi, K. Krakowiak, M. Bauchy, K. Stewart, R. Shahsavari, D. Jagannathan, D. Brommer, A. Baronnet, M. Buehler, K. Van Vliet *et al.*, "Concrete under the nanoscope: Combinatorial optimization by screening defect attributes," Nat. Commun. (submitted).
[15]M. Abdolhosseini Qomi, M. Bauchy, R. J.-M. Pellenq, and F.-J. Ulm, in *Mechanics and Physics of Creep, Shrinkage, and Durability of Concrete: A Tribute to Zdenek P. Bazant: Proceedings of the Ninth International Conference on Creep, Shrinkage, and Durability Mechanics (CONCREEP-9), 22–25 September* (ASCE Publications, Cambridge, MA, 2013).
[16]M. J. A. Qomi, M. Bauchy, F.-J. Ulm, and R. J.-M. Pellenq, J. Chem. Phys. **140**, 054515 (2014).
[17]S. Hamid, Z. Kristallogr. **154**, 189–198 (1981).
[18]R. J.-M. Pellenq, A. Kushima, R. Shahsavari, K. J. V. Vliet, M. J. Buehler, S. Yip, and F.-J. Ulm, Proc. Natl. Acad. Sci. U.S.A. **106**, 16102 (2009).
[19]M. Abdolhosseini Qomi, F.-J. Ulm, and R. J.-M. Pellenq, J. Am. Ceram. Soc. **95**, 1128–1137 (2012).
[20]H. Manzano, S. Moeini, F. Marinelli, A. C. T. van Duin, F.-J. Ulm, and R. J.-M. Pellenq, J. Am. Chem. Soc. **134**, 2208 (2012).
[21]M. Bauchy, M. A. Qomi, R. J. M. Pellenq, and F. J. Ulm, *Computational Modelling of Concrete Structures* (CRC Press, 2014), p. 169.
[22]S. Plimpton, J. Comput. Phys. **117**, 1–19 (1995).
[23]M. Bauchy, M. Micoulaut, M. Celino, S. Le Roux, M. Boero, and C. Massobrio, Phys. Rev. B **84**, 054201 (2011).
[24]R. C. Weast, Am. J. Med. Sci. **257**, 423 (1969).
[25]M. Bauchy and M. Micoulaut, J. Non-Cryst. Solids **357**, 2530 (2011).
[26]K. Vollmayr, W. Kob, and K. Binder, Phys. Rev. B **54**, 15808 (1996).
[27]L. Cormier, D. R. Neuville, and G. Calas, J. Am. Ceram. Soc. **88**, 2292–2299 (2005).
[28]M. Bauchy, J. Chem. Phys. **137**, 044510 (2012).
[29]M. Micoulaut, A. Kachmar, M. Bauchy, S. Le Roux, C. Massobrio, and M. Boero, Phys. Rev. B **88**, 054203 (2013).
[30]S. Soyer-Uzun, S. R. Chae, C. J. Benmore, H.-R. Wenk, and P. J. M. Monteiro, J. Am. Ceram. Soc. **95**, 793–798 (2012).
[31]M. Bauchy, "Structural, vibrational, and elastic properties of a calcium aluminosilicate glass from molecular dynamics simulations: The role of the potential," preprint arXiv:1403.1640 [cond-mat] (2014).
[32]A. C. Wright, J. Non-Cryst. Solids **159**, 264 (1993).
[33]A. C. Wright, J. Non-Cryst. Solids **106**, 1 (1988).
[34]J. Du and L. R. Corrales, J. Non-Cryst. Solids **352**, 3255 (2006).
[35]V. F. Sears, Neutron News **3**, 26 (1992).
[36]M. Micoulaut and M. Bauchy, Phys. Status Solidi B **250**, 976–982 (2013).
[37]M. Bauchy, M. Micoulaut, M. Boero, and C. Massobrio, Phys. Rev. Lett. **110**, 165501 (2013).
[38]A. Baranyai and D. J. Evans, Phys. Rev. A **40**, 3817 (1989).
[39]M. Bauchy, B. Guillot, M. Micoulaut, and N. Sator, Chem. Geol. **346**, 47 (2013).